

# EGRET search for three recently-discovered radio pulsars

D.Parent<sup>1</sup>, L. Guillemot<sup>1</sup> and D.A. Smith<sup>1</sup>

## ABSTRACT

We present a search for pulsed gamma-ray emission in the EGRET data from three recently-discovered radio pulsars, J1410–6132 discovered at Parkes, and J2240+5832 and J0248+6021 discovered at Nançay. No pulsed gamma-ray emission has been detected, despite spin-down energies from  $2 \times 10^{35}$  ergs/s to  $1 \times 10^{37}$  and their proximity to the unidentified EGRET sources 3EG J1410–6147 and 3EG J0241+6103. The analysis was limited by the low statistics and the large time interval between the observations by EGRET and the radio observations, which provide the ephemerides, although we successfully detected the known  $\gamma$ -ray pulsars B0833–45 and B1706–44 with our method. We also discuss the possible  $\gamma$ -ray emission of these pulsars. GLAST will offer us the possibility to repeat this analysis with more events and up-to-date radio ephemerides.

*Subject headings:* gamma rays: general; pulsars: individual: J1410–6132, J2240+5832, J0248+6021

## 1. Introduction

Pulsars are expected to stop being gamma-ray emitters ( $> 100$  MeV) when the spin-down energy  $\dot{E}$  falls below  $3 \times 10^{34}$  ergs/s (Guillemot et al. 2008). Since the end of the EGRET mission, the number of gamma-ray candidates among radio pulsars increased from  $\sim 60$  to a hundred (see ATNF). However, all *a posteriori* pulsation searches have been unsuccessful (see for example the cases of the radio pulsars J2229+6114 (Thompson et al. 2002), B0656+14 (Ramanamurthy et al. 1996) and B1046–58 (Kaspi et al. 2000)). The Parkes radio observatory recently discovered the pulsar J1410–6132, and the Nançay radio telescope discovered J0248+6021 and J2240+5832 (Ray et al. 1999), in the Foster et al. survey in the years 1997-1999. Details on these objects are listed in Table 1. Their spin-down energy rates exceed  $2 \times 10^{35}$  ergs/s, making them new gamma-ray pulsar candidates.

---

<sup>1</sup>CENBG

Table 1: Observed and computed radio parameters

JName	P (ms)	$\dot{E}$ (erg s <sup>-1</sup> )	(l,b) (°)	d (kpc)	$\tau$ (ky)	$\sqrt{\dot{E}/d^2}$
J1410–6132	50.1	$1.0 \times 10^{37}$	312.20,–0.09	15.115	25	$1.38 \times 10^{16}$
J2240+5832	139.9	$2.2 \times 10^{35}$	106.57,–0.11	10.402	145	$4.3 \times 10^{15}$
J0248+6021	217.1	$2.1 \times 10^{35}$	136.90,+0.70	12.5	62	$2.95 \times 10^{15}$

Note.  $\tau = P/2\dot{P}$ , and  $\dot{E} = 4 \pi^2 I \dot{P}/P^3$  with  $I = 45 \text{ g cm}^2$ . Distances  $d$  were computed with the NE2001 electron density model (Taylor et al.). The distance of J0248+6021 is discussed by Cognard et al.

In this note, we present a method for periodicity search, its validation with the known  $\gamma$ -ray pulsars B0833–45 and B1706–44 and its application to three radio pulsars. We finally discuss the possibility of  $\gamma$ -ray emission from PSR J1410–6132 and PSR J0248+6103.

## 2. Observations

The analyzed data were recorded by the EGRET detector, described by Thompson et al. (1993) and stored by observatory operating phase and viewing periods (VP). In Table 3, we list the selected EGRET viewing periods for the three pulsars. The energy-dependent angular resolution of the EGRET instrument is given by (Thompson et al. 1993):

$$\theta_{0.67} \geq 5.85^\circ (E_\gamma/100 \text{ MeV})^{-0.534}. \quad (1)$$

We selected the data in three energy ranges  $>100 \text{ MeV}$  to keep an almost complete data set, 100-300 and  $>300 \text{ MeV}$  respectively interesting in the case of a pulsar with a relatively low energy cut-off and spectral hardness comparable to that of the  $\gamma$ -ray pulsar B1951+32.

Table 2: EGRET viewing periods used in this study

JName	Viewing Period	Start Date	End Date	Pointing Direction	Off-axis angle	Effective Exposure		Neuts		
		TJD	TJD	(l,b) ( $^{\circ}$ )	( $^{\circ}$ )	(100-300 MeV; $cm^2s$ )	>100 MeV	100-300 MeV	300-1000 MeV	
J0248+6021	vp0150	8588	8602	(152.63,-13.44)	21.08	$6.05 \times 10^8$	625	508	117	
	vp0310	8784	8798	(157.60, 10.01)	22.62	$6.05 \times 10^8$	282	232	50	
	vp2110	9043	9055	(125.86,-4.70)	12.28	$1.04 \times 10^9$	693	555	138	
	vp3250	9468	9482	(146.36, -7.93)	12.79	$1.21 \times 10^9$	586	456	130	
	vp5300	10332	10359	(126,2.46)	11.04	$2.33 \times 10^9$	423	293	130	
J1410-6132	vp0120	8546	8560	(310.71,22.21)	22.35	$6.05 \times 10^8$	857	687	170	
	vp0140	8574	8588	(285.04,-0.74)	27.17	$3.63 \times 10^8$	557	468	89	
	vp0230	8700	8714	(322.14,3.01)	10.41	$1.21 \times 10^9$	610	468	142	
	vp0270	8740	8749	(332.24,2.52)	20.21	$3.89 \times 10^8$	355	252	83	
	vp3140	9355	9368	(304.18,-0.99)	8.07	$1.12 \times 10^9$	831	616	215	
	vp3150	9368	9375	(304.18,-0.99)	8.07	$6.05 \times 10^8$	421	310	111	
	vp3160	9375	9384	(309.52,19.42)	19.69	$3.89 \times 10^8$	336	242	94	
J2240+5832	vp0340	8819	8840	(108.75,-2.37)	3.12	$1.81 \times 10^9$	233			

Note. TJD = JD - 2440000.5 = MJD - 40000. TJD = 8588 refers to November 11, 1991.

Start and End dates are taken from the third EGRET catalog (Hartman et al. 1999), as well as the pointing directions in galactic coordinates. The effective exposure is the product of the integration time and the effective area, which is taken from Thompson et al., 1993.

### 3. EGRET periodicity search

#### 3.1. Analysis

From radio ephemerides which are not contemporaneous to EGRET viewing periods, the rotational frequency  $\nu$  and the first-derivative  $\dot{\nu}$  have been extrapolated to the VP time. Young pulsars are characterized by glitches and timing noise. Hence, timing ephemerides can become inaccurate within weeks to months for many of the best gamma pulsar candidates (Arzoumanian et al.1994). It was necessary to evaluate the search intervals in  $\nu$  and  $\dot{\nu}$ , and the incrementation steps on these parameters, while limiting the number of trials.

To test the periodicity, we built a lightcurve for each pair of  $\nu$  and  $\dot{\nu}$  and calculated the fluctuation detection probability using the standard  $\chi^2$  method (note 1 below) and the bin-independent H-test (De Jager) which both depend on the pulse shape. The rotational parameters are included in intervals centered on the extrapolated frequency and derivative (note 2), and the size of steps is a function of the unknown  $\gamma$  peak width (note 3). The final fluctuation detection probability is corrected for the number of trials (note 4).

- [1]  $\chi^2$  estimates the deviation from a flat distribution with  $\langle n \rangle = N/nbin$  (with N is the total number of events) in each bin and is defined by:

$$\chi^2 = \sum_{i=1}^{nbin} \frac{(n_i - \langle n \rangle)^2}{n_i}, \quad (2)$$

with  $n_i$  the number of events at each bin of the phasogram. From the  $\chi^2$  and the number of degrees of freedom ( $nbin - 1$ ), we calculate a fluctuation detection probability. For a number of trials  $N_{trials}$ , this probability is given by:

$$P_{tot} = 1 - (1 - P_{one\ trial})^{N_{trials}} \quad (3)$$

with  $P_{one\ trial}$  the probability associated to the best detection. As an example, Figure 1 gives a  $\chi^2$  of 9.80 with 9 degrees of freedom, and a fluctuation detection probability of  $\sim 0.3667$  (confidence intervals for a  $\chi^2$  distribution) for one trial. If we assume that this detection is the best one among 10 trials, this probability becomes  $\sim 0.9896$ .

- [2] In order to estimate the search intervals  $\delta\nu_{psr}$  and  $\delta\dot{\nu}_{psr}$ , we used Jodrell's ephemerides for the young and noisy Crab pulsar (<ftp://ftp.jb.man.ac.uk/pub/psr/crab/all.gro>). We note that the largest time interval between EGRET data and the reference epoch in our ephemerides for J1410–6132 is  $\sim 16$  years. Hence, we extrapolated the Crab pulsar  $\nu$  and  $\dot{\nu}$  from their values at time 54328 MJD to 48545 MJD,  $\sim 16$  years in

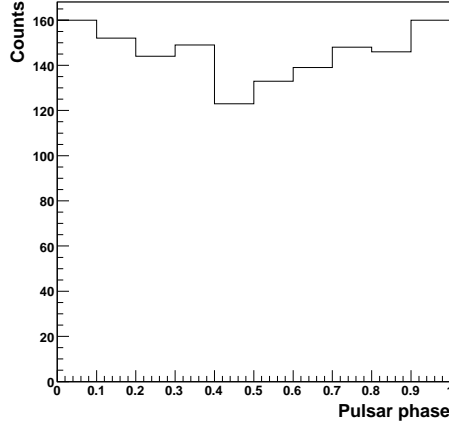


Fig. 1.—  $\chi^2$  analysis of the EGRET background. The  $\chi^2$  is 9.80 with 9 degrees of freedom, and a fluctuation detection probability of  $\sim 0.3667$  for one trial.

the past, and compared with the actual ephemeris given by Jodrell. The differences between radio rotational parameters were used to estimate the upper and lower limits on the frequency and the first derivative as standards for the following studies (Table 3). From this, we define the search intervals by:

$$\nu_{psr} \pm \delta\nu_{psr} = \nu_{psr} \pm \left(10^{-3} \times \frac{\nu_{psr}}{\nu_{Crab}}\right) \quad (4)$$

$$\dot{\nu}_{psr} \pm \delta\dot{\nu}_{psr} = \dot{\nu}_{psr} \pm \left(5 \times 10^{-2} \times \frac{\dot{\nu}_{psr}}{\dot{\nu}_{Crab}}\right) \quad (5)$$

We note that the actual frequency and derivative is out of the uncertainty interval extrapolated to the past.

Table 3: Difference extrapolated and observed rotation parameters for the Crab

Rotational parameters	54328.000000250 MJD	48545.000000253 MJD	Difference (Obs–Ext)
$\nu_{obs}$ ( $s^{-1}$ )	$29.7563165504927 \pm 2 \times 10^{-10}$	$29.9435753170126 \pm 1 \times 10^{-10}$	
$\nu_{ext}$ ( $s^{-1}$ )		$29.94192359681 \pm 2 \times 10^{-7}$	$\sim 1 \times 10^{-3}$
$\dot{\nu}_{obs} \times 10^{-10}$ ( $s^{-2}$ )	$-3.72282 \pm 4.4 \times 10^{-6}$	$-3.77479 \pm 3.4 \times 10^{-6}$	
$\dot{\nu}_{ext} \times 10^{-10}$ ( $s^{-2}$ )		$-3.72467 \pm 3.4 \times 10^{-6}$	$\sim 5 \times 10^{-2}$

[3] The lightcurves of most  $\gamma$ -ray pulsars show two peaks separated of 0.4 in phase with a peak width of  $\sim 0.1$ . From those observations, we chose to build 10 bin histograms, that is,  $\Delta\phi = 0.1$ , to maximize the statistics in the peak. In order to estimate the frequency and derivative steps, we imposed that the farthest event from the reference

epoch of the ephemeris could be shifted by 0.1 in phase at maximum. Hence, we define the increment steps by

$$\Delta\nu = \frac{\Delta\phi_{max}}{t_{farthest} - t_0} = \frac{0.1}{t_{farthest} - t_0}, \quad (6)$$

$$\Delta\dot{\nu} = \frac{2 \times \Delta\phi_{max}}{(t_{farthest} - t_0)^2} = \frac{0.2}{(t_{farthest} - t_0)^2} \quad (7)$$

with  $t_0$  the ephemeris reference epoch and  $t_{farthest}$  is the farthest time from the reference epoch of the ephemeris.

[4] The number of trials  $N_{trials}$  is defined by:

$$N_{trials} = \left( \frac{\nu_{max} - \nu_{min}}{\Delta\nu} \times \frac{\dot{\nu}_{max} - \dot{\nu}_{min}}{\Delta\dot{\nu}} \right), \quad (8)$$

with  $\nu_{max} = \nu + \delta\nu_{psr}$  and  $\nu_{min} = \nu - \delta\nu_{psr}$  and  $\dot{\nu}_{max} = \dot{\nu} + \delta\dot{\nu}_{psr}$  and  $\dot{\nu}_{min} = \dot{\nu} - \delta\dot{\nu}_{psr}$ .

We will apply the search method on the viewing periods with a number of events exceeding 200. To validate a detection, the rotational parameters determined from one data set should confirm a consistent signal from the other independent data sets, that is high statistical significance for both lightcurve and similar pulse profiles.

### 3.2. Validation with B0833–45 and B1706–44

In order to validate the pulsation search, we applied our analysis to both  $\gamma$ -ray pulsars B0833–45 and B1706–44, detected during the EGRET mission.

PSR B0833–45 (Vela) is the brightest source of the  $\gamma$ -ray sky with a flux of  $(7.8 \pm 1.0) \times 10^{-6}$  photons  $\text{cm}^{-2} \text{s}^{-1}$  between 100 MeV and 2 GeV (Kanbach et al. 1994). The  $\gamma$ -ray pulse profile shows 2 peaks separated by 0.42 in phase. We used the data in VP0007, starting at MJD 48386 and ending at MJD 48392, and the ephemerides presented in Table 4 (Strickman et al. 1999), which is 5.6 years after the event times.

We extrapolated the radio ephemerides from 50440 MJD to 48386 MJD (VP0007) and phase folded event times with each pair of  $\nu$  and  $\dot{\nu}$  with the following search intervals and steps:

$$\begin{aligned} [\nu_{min}, \nu_{max}] &= 11.1989570255396 \pm (10^{-3} \times \frac{11.1989570255396}{29.9435753170126}) = [11.1986; 11.1993], \\ [\dot{\nu}_{min}, \dot{\nu}_{max}] &= -1.6247695 \times 10^{-11} \pm (5 \times 10^{-12} \times \frac{-1.6247695 \times 10^{-11}}{-3.77479 \times 10^{-10}}) = [-1.84 \times 10^{-11}; -1.41 \times 10^{-11}], \\ \Delta\nu &= \frac{\Delta\phi_{max}}{t_{farthest} - t_0} = \frac{0.1}{(48392 - 48386) \times 86400} = 2 \times 10^{-7}, \end{aligned}$$

$$\Delta\dot{\nu} = \frac{2 \times \Delta\phi_{max}}{(t_{farthest} - t_0)^2} = \frac{0.2}{((48392 - 48386) \times 86400)^2} = 7 \times 10^{-13},$$

$$N_{trials} = \left(\frac{11.1993 - 11.1986}{2 \times 10^{-7}}\right) \times \frac{-1.41 \times 10^{-11} + 1.84 \times 10^{-11}}{7 \times 10^{-13}} = 22427$$

The most probable detection was for  $\nu = 11.1988296255396$  with  $E > 100$  MeV, with the probability of  $4.48 \times 10^{-95}$  (for a  $\chi^2$  distribution) to detect a fluctuation. Figure 2 shows the  $\chi^2$  values for a frequency distribution with constant first-derivative, which rules out the null hypothesis (left) and the 10 bin phasogram for B0833-45 with the reconstructed rotational parameters and an arbitrary absolute phase (right). The result is very similar to that presented by Kanbach et al (1994).

Table 4: Vela pulsar ephemerides

Parameter	Value	Extrapolated Value	Reconstructed Value
Epoch (MJD)	50440.000000226	48386	48386
$\nu$ (s <sup>-1</sup> )	11.1961237576948	11.1989570255396	11.1988296255396
$\dot{\nu}$ (s <sup>-2</sup> )	$-1.56671 \times 10^{-11}$	$-1.6247695 \times 10^{-11}$	$-1.55998 \times 10^{-11}$
$\ddot{\nu}$ (s <sup>-3</sup> )	$3.27 \times 10^{-21}$	$3.27 \times 10^{-21}$	$3.27 \times 10^{-21}$
Epoch (MJD)	50440.000000226	48490	48490
$\nu$ (s <sup>-1</sup> )	11.1961237576948	11.1988097610126	11.1987193610126
$\dot{\nu}$ (s <sup>-2</sup> )	$-1.56671 \times 10^{-11}$	$-1.621803 \times 10^{-11}$	$-1.570623249 \times 10^{-11}$
$\ddot{\nu}$ (s <sup>-3</sup> )	$3.27 \times 10^{-21}$	$3.27 \times 10^{-21}$	$3.27 \times 10^{-21}$

Note. The Table presents the starting ephemeris, the extrapolated ephemeris and the reconstructed ephemeris, for the viewing periods VP0007 (48386 MJD) and VP0080 (48490).

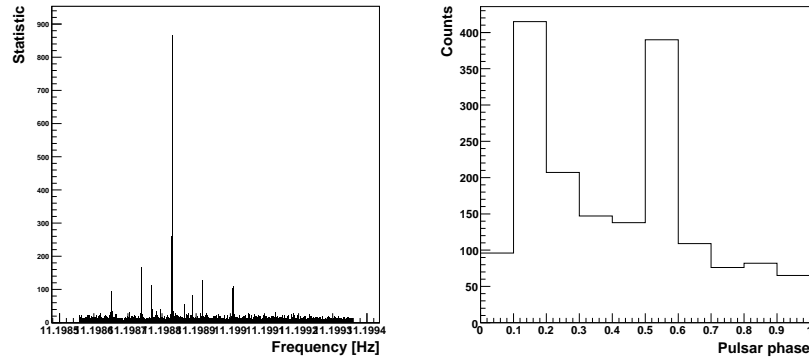


Fig. 2.— LEFT.  $\chi^2$  values obtained for the Vela pulsar. The maximum value is obtained for  $\nu = 11.1988296255396$  s<sup>-1</sup> and  $\dot{\nu} = -1.55998 \times 10^{-11}$  s<sup>-2</sup> with the fluctuation detection probability ( $P_{one\ trial}$ ) =  $8.15 \times 10^{-96}$  (3700 trials on the frequency with a constant first-derivative). RIGHT. Vela light curve for VP0007, based on the  $\nu$  and  $\dot{\nu}$  determined by the periodicity search from extrapolated radio ephemerides. The data consists of 1725 events with  $E > 100$  MeV. The absolute phase is arbitrary.

In the second step, we applied the new ephemeris obtained with VP0007 (Table 4) on 4 other viewing periods (Figure 3). We didn't confirm a consistent signal. We note that the time interval between VP0007 and the next viewing periods is  $> 70$  days. Hence, it was necessary to apply a new periodicity search on the other VP and to compare the lightcurves. Figure 4 presents the results of a new periodicity search from the viewing period 80 and Table 5 summarizes the results. The lightcurve is identical to the viewing period 07. We confirm the detection of the Vela  $\gamma$ -ray pulsar. We did not apply the periodicity search on the other viewing periods because the detection was confirmed.

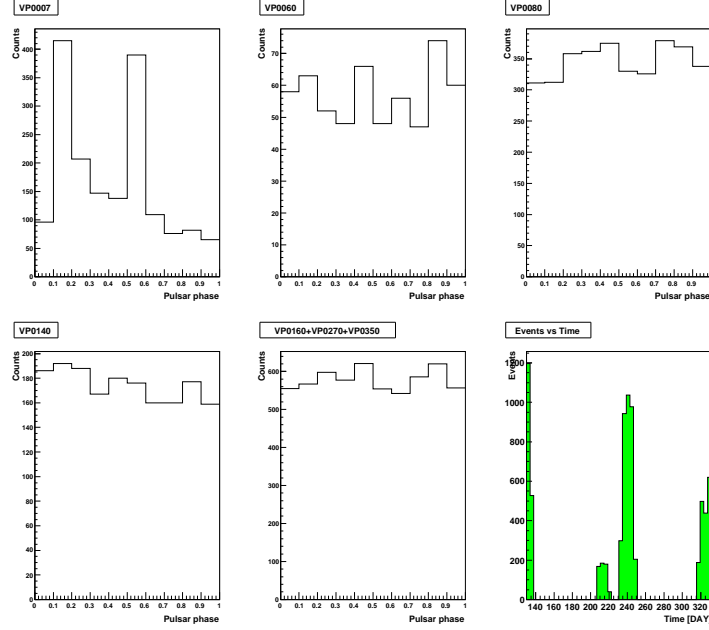


Fig. 3.— Lightcurves of the Vela pulsar from the new ephemeris obtained with VP0007 (Table 4).

Table 5: Confidence levels for B0833–45

Viewing period	Confidence levels
0007	$4.48 \times 10^{-95}$
0080	$1.83 \times 10^{-95}$

Note. The Table presents the confidence levels for a  $\chi^2$  distribution (fluctuation detection probability).

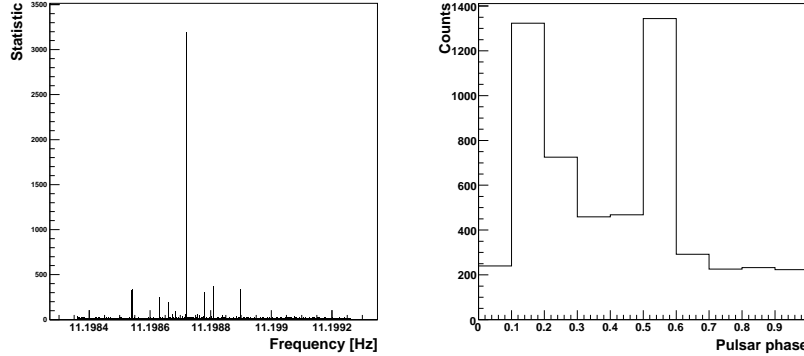


Fig. 4.— LEFT.  $\chi^2$  values obtained for the Vela pulsar for VP0080. The maximum value is obtained for  $\nu = 11.1987193610126 \text{ s}^{-1}$  and  $\dot{\nu} = -1.5706 \times 10^{-11} \text{ s}^{-2}$  with the fluctuation detection probability ( $P_{one \text{ trial}} = 1.85 \times 10^{-95}$  (9000 trials on the frequency with a constant first-derivative). RIGHT. Vela lightcurve, based on the  $\nu$  and  $\dot{\nu}$  determined by the periodicity search from extrapolated radio ephemerides. The data consists of 5532 events with  $E > 100 \text{ MeV}$ . The absolute phase is arbitrary.

PSR B1706–44 was detected by EGRET (Nolan et al.) with a  $\gamma$ -ray flux of  $(1.28 \pm 0.08) \times 10^{-6} \text{ photons cm}^{-2} \text{ s}^{-1}$  ( $E > 100 \text{ MeV}$ ) (fourth flux after Vela, Geminga and Crab). The pulse profile consists in three pulses, and no unpulsed emission has been observed. Starting from the ephemerides presented in Table 6 and search parameters in Table 7, we searched for pulsation in the VP0050 data (number of events  $> 200$ ) starting at MJD 48449 and ending at MJD 48463. The time interval between the radio ephemerides and the data is  $\sim 16$  years. The best signal was detected for  $\nu = 9.761253358993 \text{ s}^{-1}$  and  $E > 300 \text{ MeV}$ . Taking into account the number of trials, the fluctuation detection probability obtained is of  $6 \times 10^{-3}$ . Figure 5 shows both the  $\chi^2$  values for a frequency distribution with constant first-derivative, and the VP0050 lightcurve using the reconstructed rotational parameters presented in Table 6. The results are very similar to those presented by Thompson et al. (1996).

In the second step, we applied the new ephemeris on the viewing periods VP0160, VP270 and VP0350. We calculated the fluctuation detection probability for the distribution (VP0160+VP270+VP0350) shown in Figure 6. Though we made only one trial, we found the probability of  $9 \times 10^{-3}$  for 9 degrees of freedom. We didn't confirm a consistent signal. We note that the time interval between VP0050 and the others is exceeding 100 days. It might result from glitches and timing noise that are features of  $\gamma$ -ray pulsars.

However, we searched the periodicity for the VP 3230 (235 events), and detected a signal for  $\nu = 9.761253358993 \text{ s}^{-1}$  and  $E > 300 \text{ MeV}$ , with a fluctuation detection probability of  $1 \times 10^{-4}$ . Figure 7 presents the  $\chi^2$  distribution and the lightcurve, which is similar to the VP0050. This result allows the confirmation of the PSR B1706–44 detection. We note also that we didn't confirm a consistent signal from the closer viewing periods. The difficulty to

Table 6: Radio ephemeris for PSR B1706–44 (taken from Johnston et al.). The ephemerides of B1706–44 are not published yet (only few digits are shown).

Parameter	Value	Extrapolated value	Reconstructed value
Epoch (MJD)	54326	48449	48449
$\nu$ (s <sup>-1</sup> )	9.7567...	9.761253358993	9.761178758993
$\dot{\nu}$ (s <sup>-2</sup> )	-8.8439..... × 10 <sup>-12</sup>	-8.93186801545826 × 10 <sup>-12</sup>	-8.914962 × 10 <sup>-12</sup>
$\ddot{\nu}$ (s <sup>-3</sup> )	1.731 × 10 <sup>-22</sup>	1.731 × 10 <sup>-22</sup>	1.731 × 10 <sup>-22</sup>
Epoch (MJD)	54326	49433	49433
$\nu$ (s <sup>-1</sup> )	9.7567...	9.7604938481523	9.7604444481523
$\dot{\nu}$ (s <sup>-2</sup> )	-8.8439..... × 10 <sup>-12</sup>	-8.91713 × 10 <sup>-12</sup>	-9.015 × 10 <sup>-12</sup>
$\ddot{\nu}$ (s <sup>-3</sup> )	1.731 × 10 <sup>-22</sup>	1.731 × 10 <sup>-22</sup>	1.731 × 10 <sup>-22</sup>

Note. The Table presents the starting ephemeris, the extrapolated ephemeris and the reconstructed ephemeris, for the viewing periods VP0050 (48449 MJD) and VP3230 (49433).

Table 7: B1706–44 search parameters for VP0007 at the 48449 MJD reference epoch.

Parameter	Value	Lower limit	Upper limits	Step
$\nu$ (s <sup>-1</sup> )	9.761253358993	9.76092737075493	9.76157934723107	1 × 10 <sup>-7</sup>
$\dot{\nu}$ (s <sup>-2</sup> )	-8.93186801545826 × 10 <sup>-12</sup>	-10.114962 × 10 <sup>-12</sup>	-7.7487733 × 10 <sup>-12</sup>	1.4 × 10 <sup>-13</sup>

Note. The number of trials from those parameters is 187200.

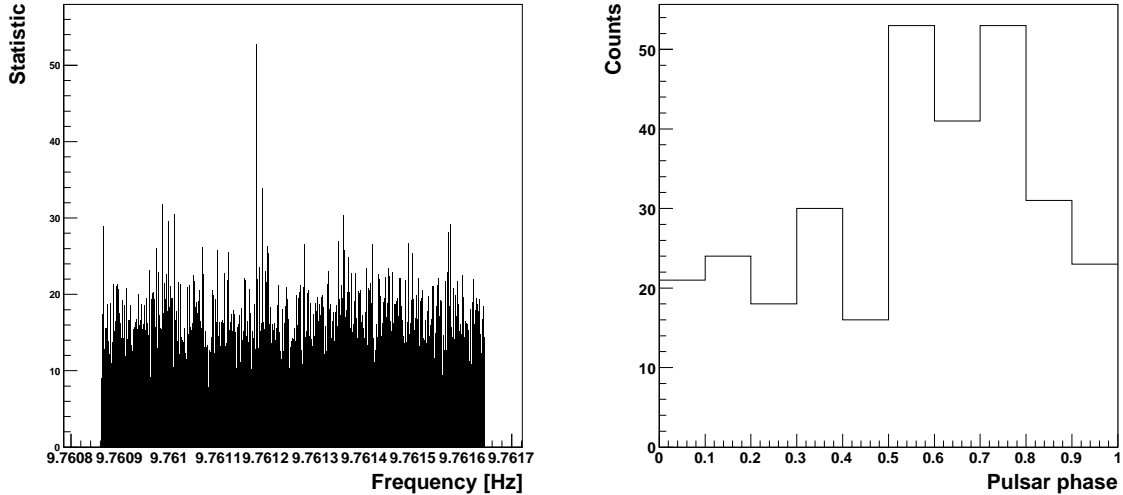


Fig. 5.— LEFT.  $\chi^2$  values obtained for the vp0050 of B1706–44. The confidence levels is  $6 \times 10^{-3}$  for 187,200 trials at  $\nu_0 = 9.761178758993$  s<sup>-1</sup> and  $\nu_1 = -8.914962 \times 10^{-12}$  s<sup>-2</sup>. RIGHT. B1706–44 light curve in Viewing Period 0050, based on the frequency and derivatives determined by the periodicity search from radio ephemerides. The data consists of 301 events with E>300 MeV. The absolute phase is arbitrary.

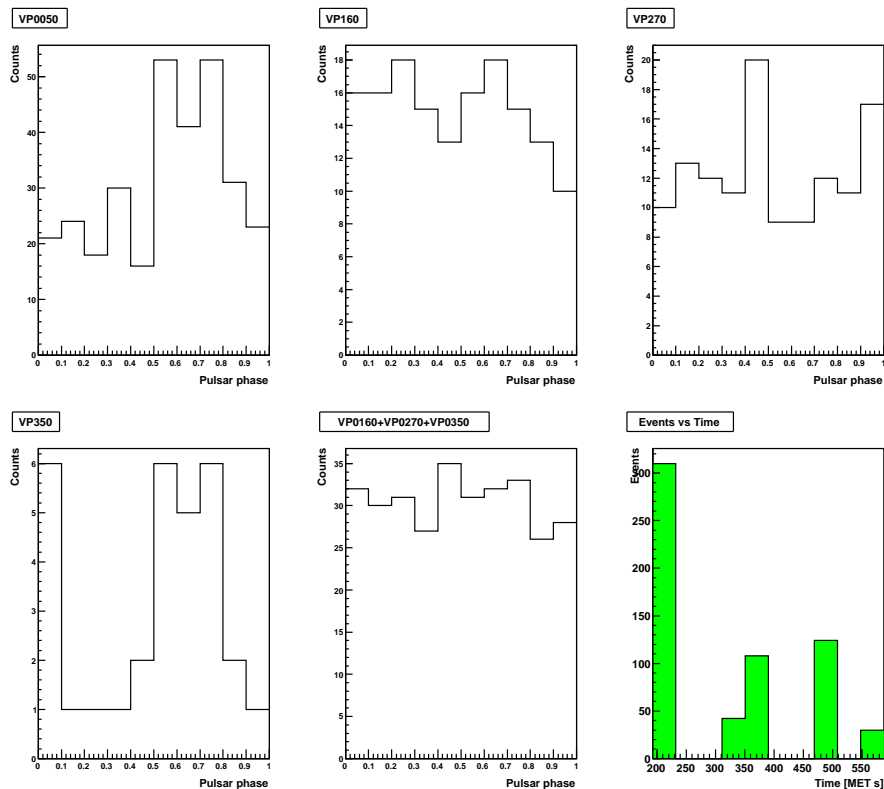


Fig. 6.— Lightcurves of B1706–44 from the new ephemeris obtained with VP0050 (Table 6).

extrapolate ephemerides illustrates the need for a datation campaign for GLAST.

Table 8: Confidence levels for B1706–44

Viewing period	Confidence levels
0050	$6 \times 10^{-3}$
3230	$1 \times 10^{-4}$

Note. The Table presents the confidence levels for a  $\chi^2$  distribution (fluctuation detection probability).  $1 \times 10^{-4}$  is a reference for the detection.

In conclusion, we validated the method for periodicity search with the two known  $\gamma$ -ray pulsars B0833–45 and B1706–44, along with search parameters. The main goal is to detect a signal with a fluctuation detection probability  $\leq 1 \times 10^{-4}$  and confirm this detection making comparisons between lightcurves.

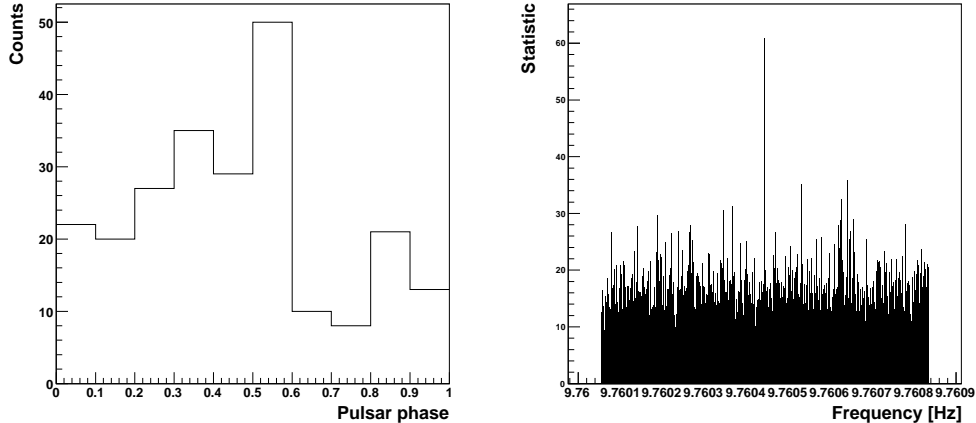


Fig. 7.— LEFT.  $\chi^2$  values obtained for the vp3250 of B1706–44. The chance probability is  $1.6 \times 10^{-4}$  for 180,000 trials at  $\nu_0 = 9.7604444481523 \text{ s}^{-1}$  and  $\nu_1 = -9.015 \times 10^{-12} \text{ s}^{-2}$ . RIGHT. B1706–44 light curve in VP3250, based on the frequency and derivatives determined by the periodicity search from radio ephemerides. The data consists of 235 events with  $E > 300 \text{ MeV}$ . The absolute phase is arbitrary.

### 3.3. PSR J1410–6132

With a period of  $\sim 50 \text{ ms}$  and spin-down power of  $\sim 10^{37} \text{ erg s}^{-1}$ , the young pulsar J1410–6132 described in Table 1, is positionally coincident with the unidentified gamma-ray source 3EG J1410–6147 with an angular separation of 0.23 deg. The 3rd EGRET catalog gives a spectral index of  $2.12 \pm 0.14$ , consistent with spectral indices of EGRET pulsars, ranging from 1.42 to 2.1. Furthermore, the efficiency  $\eta$  for conversion of spin-down luminosity  $\dot{E}$  into  $\gamma$ -ray luminosity  $L_\gamma$  required to explain the EGRET flux is 8.9% (Table 9), which seems reasonable compared with known  $\gamma$ -ray pulsars. However, the distance to the SNR G312.4–0.4, a possible counterpart of the 3 EG source (Hartman et al. 1999), is estimated at a lower distance limit of 6 kpc (Doherty et al. 2002). Finally, PSR J1410–6132 is a fourth reasonable candidate after J1407–6153, J1412–6145 and J1413–6141 (Torres et al.) located in the error box of 3EG J1410–6147. Figures 13 and 14 present the region around the pulsar.

We applied the periodicity search presented previously, to the data listed in Table 2, using the contemporaneous radio ephemeris listed in Table 10. Figures 10, 11 and 12 summarize both the  $\chi^2$  distribution and the lightcurves for the 7 viewing periods with  $E > 100$ ,  $100 < E < 300$  and  $E > 300 \text{ MeV}$  respectively. We note that no lightcurves are similar. In Table 11, we present the search results for each viewing period (reconstructed ephemerides and confidence levels). No signal was detected with a fluctuation detection probability  $\leq 1 \times 10^{-4}$  (confidence levels for B1706–44). Furthermore, the reconstructed  $\nu$  are distributed as

Table 9: Observed and computed gamma-ray parameters

PSR name	$\sqrt{\dot{E}}/d^2$	3EG name	$F^{3EG}$ ph cm <sup>-2</sup> s <sup>-1</sup>	$F^{3EG}$ ergs cm <sup>-2</sup> s <sup>-1</sup>	$\gamma^{3EG}$	$\Delta\theta$ (°)	$\theta$ (°)	$\eta$ (%)
J1410–6132	$1.38 \times 10^{16}$	J1410–6147	$(64.2 \pm 8.8) \times 10^{-8}$	$4.09 \times 10^{-10}$	$2.12 \pm 0.14$	0.23	0.36	8.9
J0248+6021	$2.95 \times 10^{15}$	J0241+6103	$(69.3 \pm 6.1) \times 10^{-8}$	$3.96 \times 10^{-10}$	$2.21 \pm 0.07$	1.8	0.18	277.1

Note. The  $\gamma$ -ray fluxes  $F^{3EG}$  are from the 3EG catalog (Hartman et al. 1999).  $\Delta\theta$  is the angular distance between the pulsar and the center of the 3EG source.  $\theta$  is the effective 95% confidence level radius of the 3EG source error box.  $\eta$  is the observed efficiency for conversion of spin-down luminosity  $\dot{E}$  into  $\gamma$ -ray luminosity  $L_\gamma$ :  $\eta = 4\pi f d^2 F^{3EG} / \dot{E}$ , we assumed the  $\gamma$ -ray beaming fraction  $f = 1/4\pi$ .

Table 10: PSR J1410–6132 pulsar ephemeris

Epoch (MJD)	54357.28617
$\nu$ (s <sup>-1</sup> )	19.979241229
$\dot{\nu}$ (s <sup>-2</sup> )	$-1.269 \times 10^{-11}$

fluctuations (Figure 8) around the extrapolated ephemeris.

We conclude that no pulsation was detected for the pulsar J1410–6132, despite J1410–6132 being a good candidate for  $\gamma$ -ray emission.

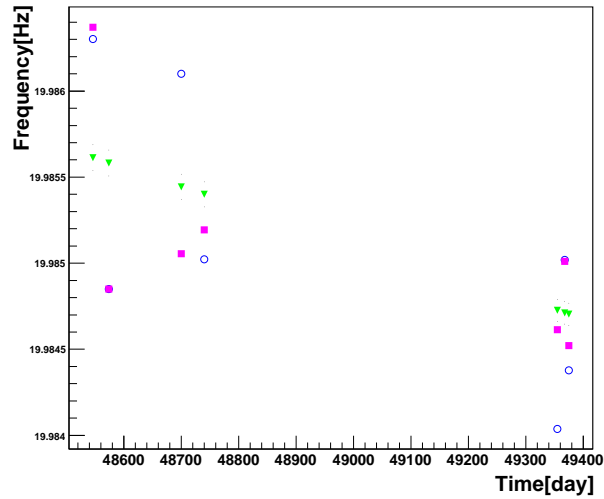


Fig. 8.— J1410–6132 - The blue and pink points represent the reconstructed  $\nu$  for  $E > 100$  MeV and  $100 < E < 300$  MeV respectively. The green points with the uncertainties represent the extrapolated ephemeris from Table 10.

Table 11: J1410–6132 pulsar ephemerides and Confidence levels

Viewing period	Parameters	Extra.Ephem	Recon.Ephem. (E>100 MeV)	Recon.Ephem. (100<E<300 MeV)	Recon.Ephem. (E>300 MeV)
120	Epoch (MJD)	48546	48546	48546	
	$\nu$ (s <sup>-1</sup> )	19.98561282	19.98630202	19.98637142	19.98615792
	$\dot{\nu} \times 10^{-11}$ (s <sup>-2</sup> )	-1.269	-1.3391	-1.1291	-1.2271
	Conf.Levels		0.5132	0.20	0.696
140	Epoch (MJD)	48574	48574		
	$\nu$ (s <sup>-1</sup> )	19.98557992	19.98485022	19.98485022	
	$\dot{\nu} \times 10^{-11}$ (s <sup>-2</sup> )	-1.269	-1.4091	-1.4091	
	Conf.Levels		0.5524	0.74	
230	Epoch (MJD)	48700	48700		
	$\nu$ (s <sup>-1</sup> )	19.98544287	19.98610037	19.98505427	
	$\dot{\nu} \times 10^{-11}$ (s <sup>-2</sup> )	-1.269	-1.18509	-1.33909	
	Conf.Levels		0.8975	0.88	
270	Epoch (MJD)	48740	48740		
	$\nu$ (s <sup>-1</sup> )	19.98539902	19.98502192	19.98519432	
	$\dot{\nu} \times 10^{-11}$ (s <sup>-2</sup> )	-1.269	-1.3171	-1.3771	
	Conf.Levels		0.5147	0.95	
3140	Epoch (MJD)	49355	49355		
	$\nu$ (s <sup>-1</sup> )	19.98472472	19.98403712	19.98461342	19.98426292
	$\dot{\nu} \times 10^{-11}$ (s <sup>-2</sup> )	-1.269	-1.3091	-1.3571	-1.1171
	Conf.Levels		0.5448	0.81	0.075
3150	Epoch (MJD)	49368	49368		
	$\nu$ (s <sup>-1</sup> )	19.98471376	19.98501876	19.98501106	
	$\dot{\nu} \times 10^{-11}$ (s <sup>-2</sup> )	-1.269	-1.10708	-1.38209	
	Conf.Levels		0.3935	0.80	
3160	Epoch (MJD)	49375	49375		
	$\nu$ (s <sup>-1</sup> )	19.98470279	19.98437829	19.98452189	
	$\dot{\nu} \times 10^{-11}$ (s <sup>-2</sup> )	-1.269	-1.1071	-1.14008	
	Conf.Levels		0.9727	0.97	

Note. This table presents the extrapolated and reconstructed ephemerides from the ephemeris of J1410–6132 (Table 10). We summarize the confidence levels (or fluctuation detection probability) for each viewing period.

### 3.4. J0248+6021

With a spin-down luminosity of  $2.1 \times 10^{35}$ , PSR J0248+6021 is considered as a  $\gamma$ -ray pulsar candidate and is a possible target for the upcoming  $\gamma$ -ray telescope GLAST. The pulsar is located  $1.8^\circ$  away from the 3EG source J0241+6103, which has a position error box at a 95% confidence level radius of only  $0.18^\circ$ . If we consider a possible association of two sources, the pulsar requires unreasonably high efficiencies exceeding 277% to explain the 3EG  $\gamma$ -ray flux (Table 9). Also, we know from  $\gamma$ -ray observations that the Be binary star LSI+61°303 is coincident with the EGRET source, which could be the combination of PSR J0248+6021 and LSI+61°303.

We applied the periodicity search presented previously, to the data listed in Table 2,

Table 12: PSR J0248+6021 pulsar ephemeris

RAJ	02:48:18.63897125
DECJ	60:21:34.3706520
Epoch (MJD)	51249.5
$\nu$ (s <sup>-1</sup> )	4.6063004229167213 $\pm$ 0.0000000000280686
$\dot{\nu}$ (s <sup>-2</sup> )	-1.168434667314 $\times 10^{-12}$ $\pm$ 1.532106183868 $\times 10^{-18}$
$\ddot{\nu}$ (s <sup>-3</sup> )	3.806407917949 $\times 10^{-24}$ $\pm$ 3.179691085405 $\times 10^{-26}$

using the contemporaneous radio ephemeris listed in Table 12. The search is centered around the pulsar position. Figures 15 and 16 summarize both the  $\chi^2$  distribution and the lightcurves for the 5 viewing periods with  $E > 100$  and  $100 < E < 300$  MeV respectively. We note that no lightcurves are similar. In Table 13, we present the search results for each viewing period (reconstructed ephemerides and confidence levels). No signal was detected with a fluctuation detection probability  $\leq 1 \times 10^{-4}$  (confidence levels for B1706-44). Furthermore, the reconstructed  $\nu$  are distributed as fluctuations (Figure 9) around the extrapolated ephemeris.

We conclude that no pulsation was detected for the pulsar J0248+6021, despite J0248+6021 being a good candidate for  $\gamma$ -ray emission.

Table 13: J0248+6021 pulsar ephemerides and Confidence levels

Viewing period	Parameters	Extra.Ephem	Recon.Ephem. (E>100 MeV)	Recon.Ephem. (100<E<300 MeV)
150	Epoch (MJD)	48588	48588	48588
	$\nu$ (s <sup>-1</sup> )	4.606569327	4.606671627	4.606744527
	$\dot{\nu} \times 10^{-12}$ (s <sup>-2</sup> )	-1.169543871	-1.051072858	-1.324458962
	Conf.Levels		0.782	0.7164
310	Epoch (MJD)	48784	48784	48784
	$\nu$ (s <sup>-1</sup> )	4.606549522	4.606677722	4.606545722
	$\dot{\nu} \times 10^{-12}$ (s <sup>-2</sup> )	-1.169479412	-1.05099986	-1.187692913
	Conf.Levels		0.7885	0.5852
2110	Epoch (MJD)	48588	48588	48588
	$\nu$ (s <sup>-1</sup> )	4.606523353	4.606432353	4.606432353
	$\dot{\nu} \times 10^{-12}$ (s <sup>-2</sup> )	-1.169394234	-1.324289504	-1.324289504
	Conf.Levels		0.4391	0.0779
3250	Epoch (MJD)	48588	48588	48588
	$\nu$ (s <sup>-1</sup> )	4.606480415	4.606342915	4.606342915
	$\dot{\nu} \times 10^{-12}$ (s <sup>-2</sup> )	-1.169254462	-1.18743816	-1.187438167
	Conf.Levels		0.03	0.271
5300	Epoch (MJD)	50332	50332	50332
	$\nu$ (s <sup>-1</sup> )	4.606393142	4.606318492	4.606268292
	$\dot{\nu} \times 10^{-12}$ (s <sup>-2</sup> )	-1.168970316	-1.10330047915841	-1.066548987
	Conf.Levels		0.542	0.999

Note. This table presents the extrapolated and reconstructed ephemerides from the ephemeris of J0248+6021 (Table 12). We summarize the confidence levels (or fluctuation detection probability) for each viewing period.

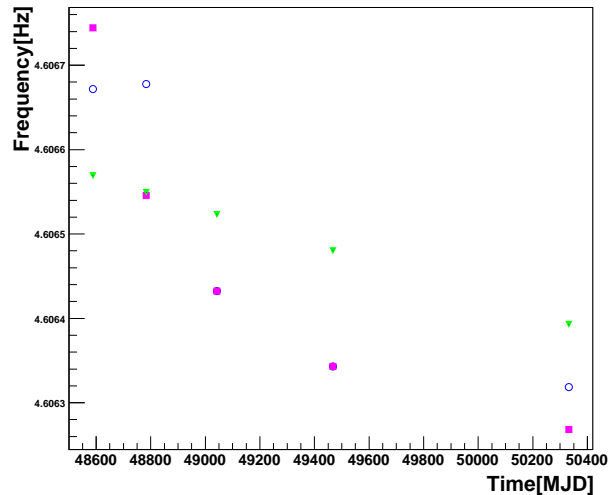


Fig. 9.— J0248+6021 - The blue circles and pink squares represent the reconstructed  $\nu$  for  $E > 100$  MeV and  $100 < E < 300$  MeV respectively. The green triangles with the uncertainties represent the extrapolated ephemeris from Table 12.

## REFERENCES

- Z. Arzoumanian et al.: ApJ 422, 671-680 (1994)
- Cognard et al. (in preparation) (2008)
- Doherty et al., Mon.Not.Roy.Astron.Soc. 339 (2003)
- Gotthelf et al., ApJ 567,125 (2002)
- Guillemot et al. ICRC (2007)
- Green et al., <http://www.mrao.cam.ac.uk/surveys/snrs/> (2006)
- Hartman, R.C., et al., ApJS, 123, 79 (1999)
- Kanbach et al., A&A 289,855 (1994)
- Johnston, S. et al.: A&A 293, 795-802 (1995)
- Kaspi et al. and Lackey J.R., ApJ 528, 445 (2000)
- Kuiper et al., A&A 359,615 (2000)
- Ramanamurthy et al., ApJ 458, 755-760 (1996)
- Ray et al. in Bulletin of the American Astronomical Society, Vol 31, p.903 (1999)

Strickman, M.S., et al., ApJ 524,373 (1999)

Taylor J. and Cordes, NE2001 (2001)

Thompson, D.J., et al., ApJS, 86, 629 (1993)

Thompson, D.J., et al., ApJ, 465, 385 (1996)

Thompson, D.J. et al. ASP Conference Series, Vol 9999 (2002)

Torres, D.F., Butt Y.M, Camilo F., ApJ 560, 155-158 (2001)

[www.atnf.csiro.au/research/pulsar/psrcat/](http://www.atnf.csiro.au/research/pulsar/psrcat/)

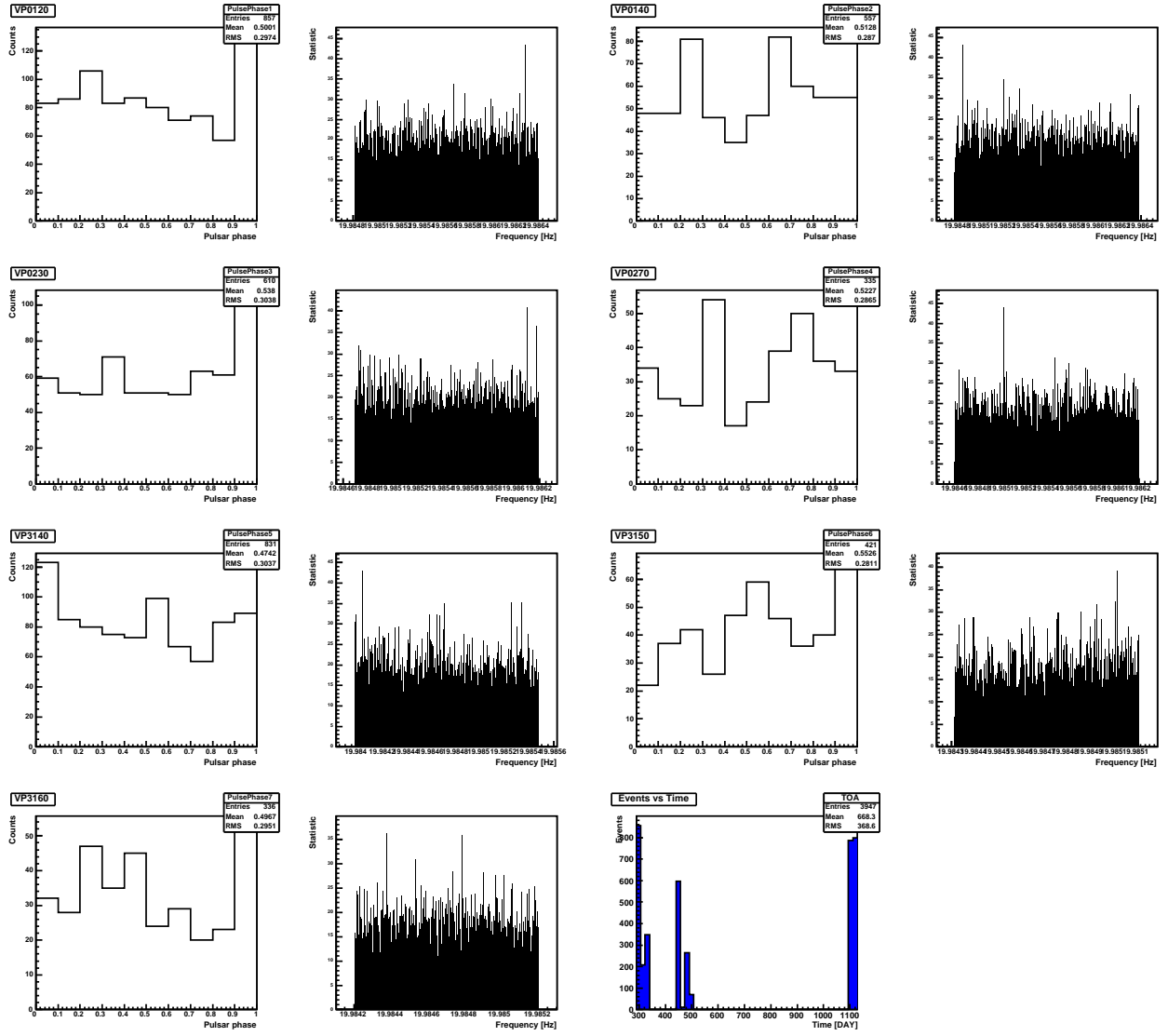


Fig. 10.—  $\chi^2$  distribution and lightcurves for J1410–6132, for the viewing periods vp0120, vp0140, vp0230, vp0270, vp3140, vp3150, vp3160 and  $E > 100$  MeV.

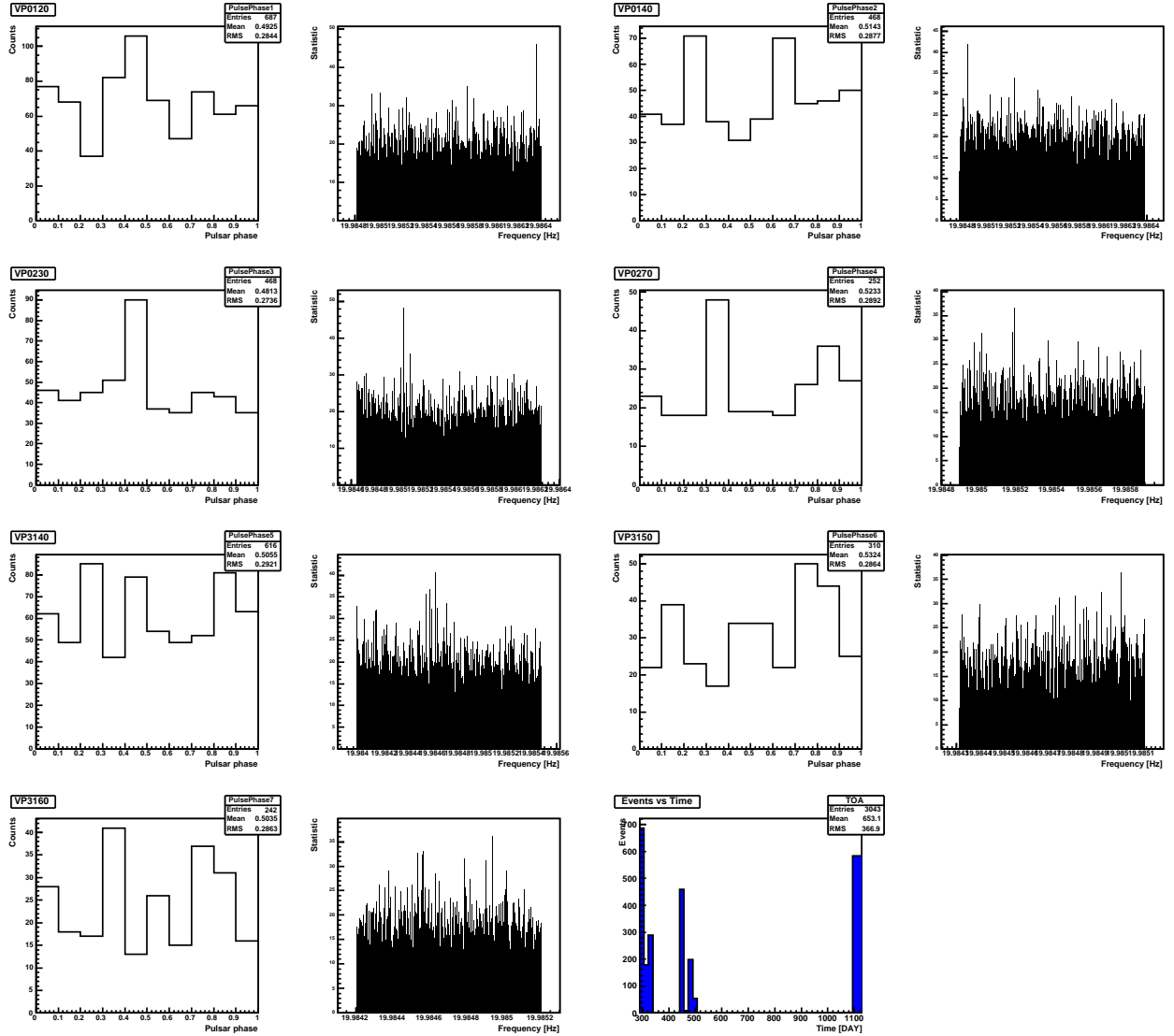


Fig. 11.—  $\chi^2$  distribution and lightcurves for J1410–6132, for the viewing periods vp0120, vp0140, vp0230, vp0270, vp3140, vp3150, vp3160 and  $100 < E < 300$  MeV.

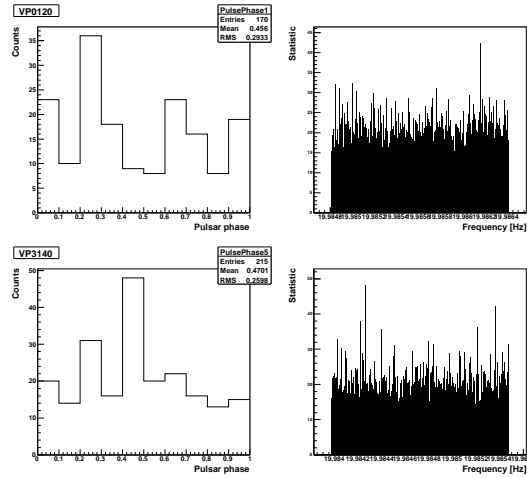


Fig. 12.—  $\chi^2$  distribution and lightcurves for J1410–6132, for the viewing periods vp0120, vp0140, vp0230, vp0270, vp3140, vp3150, vp3160 and  $E > 300$  MeV.

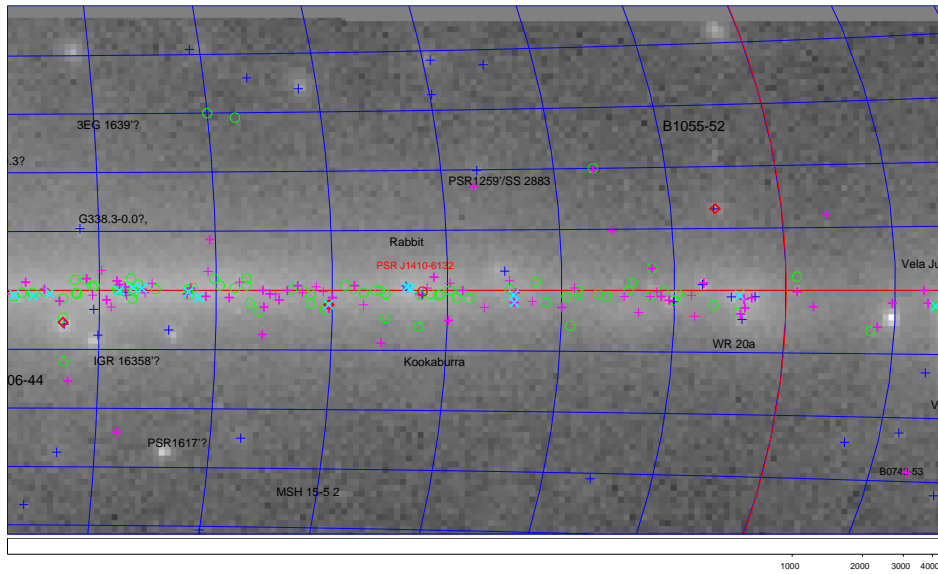


Fig. 13.—  $\gamma$ -ray sky around PSR J1410–6132. Background: simulated GLAST  $\gamma$ -ray skymap. Dark blue crosses: 3EG sources (Hartman et al., 1999). Red diamonds: EGRET detected pulsars. Green circles: galactic supernova remnants (Green, 2006). Cyan crosses: HESS detected sources. Pink crosses: radio pulsars with  $\dot{E} > 10^{34}$  ergs/s. PSR J1410–6132 is shown as a red circle.

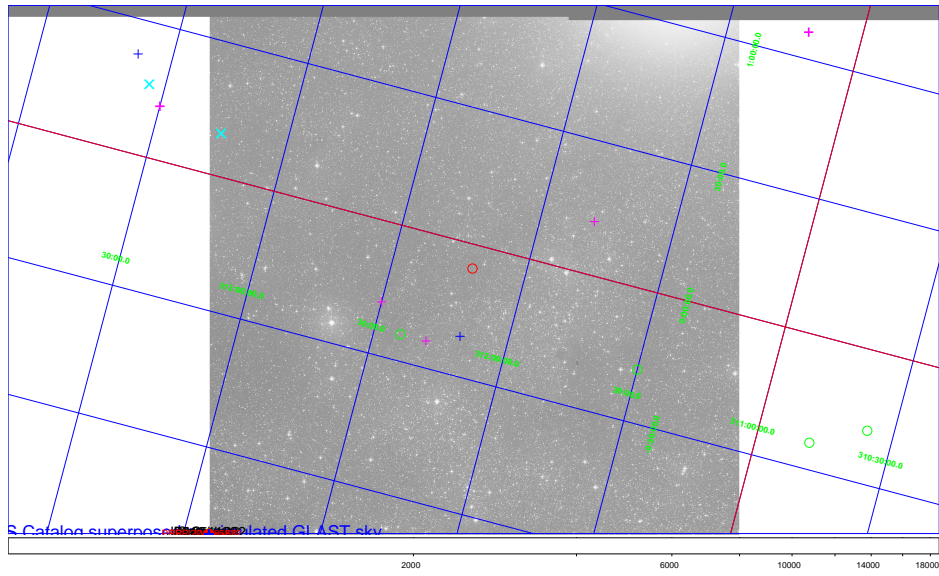


Fig. 14.— Zoom on PSR J1410–6132. Background: optical sky survey (DSS1). Contours: X-ray survey from ROSAT (RASS).

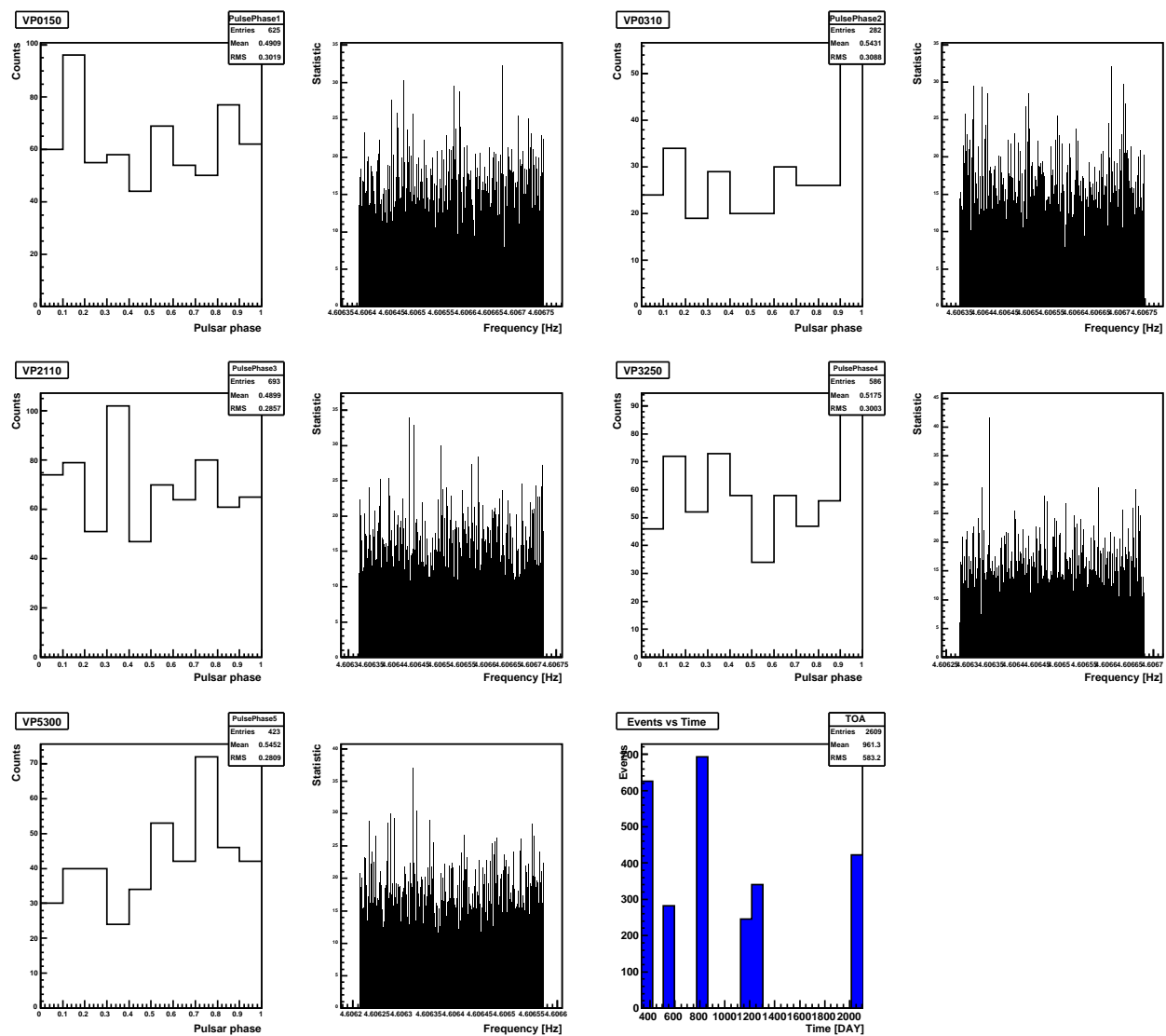


Fig. 15.—  $\chi^2$  distribution and lightcurves for J0248+6021, for the viewing periods vp0150, vp0310, vp2110, vp3250, vp5300 and  $E > 100$  MeV.

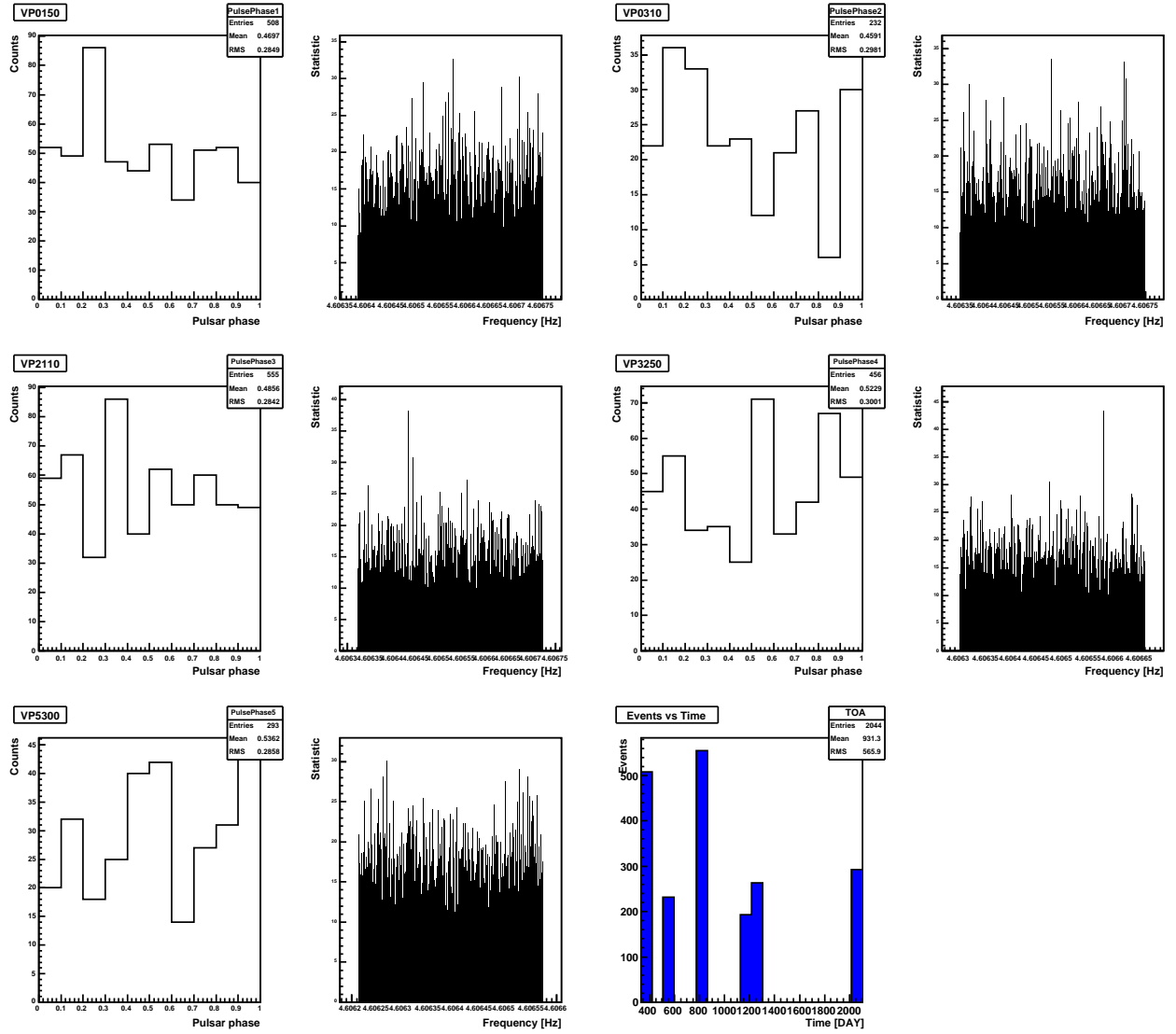


Fig. 16.—  $\chi^2$  distribution and lightcurves for J0248+6021, for the viewing periods vp0150, vp0310, vp2110, vp3250, vp5300 and  $100 < E < 300$  MeV.

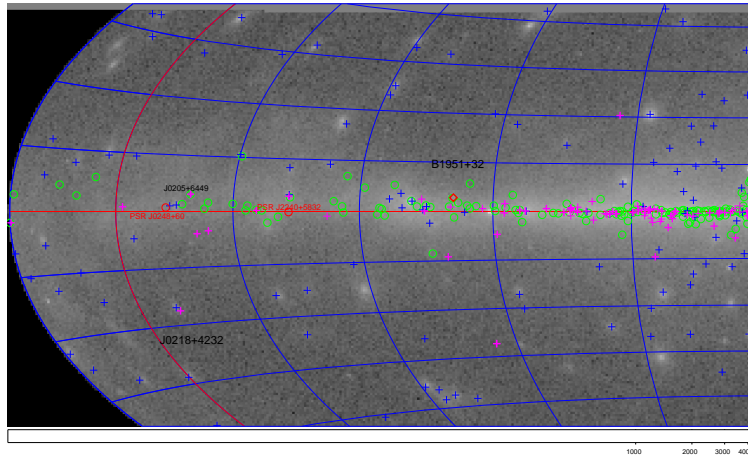


Fig. 17.— Same as Figure 13, for the region surrounding J0248+6021.

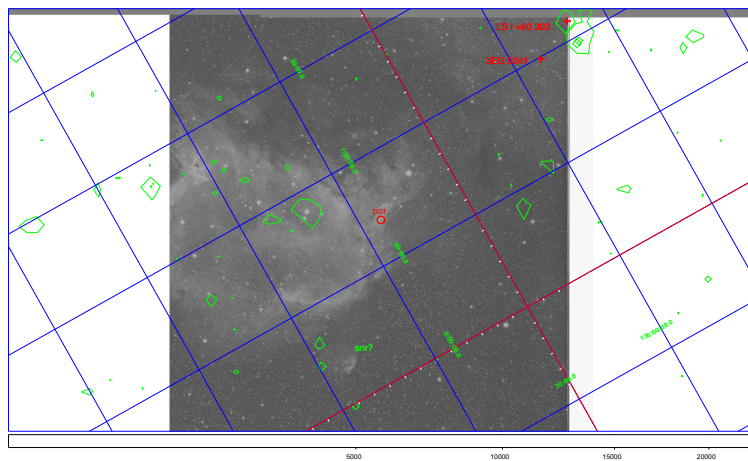


Fig. 18.— Same as Figure 14, for the region surrounding J0248+6021. The microquasar LSI+61°303 is shown on the top-right. The maximum number of X-ray events on this map, 12 events in a  $45 \times 45$  arcsec<sup>2</sup> pixel coincides with this microquasar.